

Learning-enhanced 3D fiber orientation mapping in thick cardiac tissues

Eda Nur Saruhan¹ Hakanca Ozturk² Demet Kul³ Bortecine Sevgin⁴

Merve Nur Coban⁴ Kerem Pekkan⁵

¹Computer Science and Engineering, Koç University, Rumelifeneri, Istanbul, 34450, Turkey

²Computational Science and Engineering, Imperial College, London, SW7 2AZ UK

³Cellular and Molecular Medicine, Koç University, Rumelifeneri, Istanbul, 34450, Turkey

⁴Biomedical Science and Engineering, Koç University, Rumelifeneri, Istanbul, 34450, Turkey

⁵Mechanical Engineering, Koç University, Rumelifeneri, Istanbul, 34450, Turkey

Abstract— Fibrous proteins, such as elastin and collagen, are crucial for the structural integrity of the cardiovascular system. For thin tissue-engineered heart valves and surgical patches the two-dimensional mapping of fiber orientation is well-established. However, for three-dimensional (3D) thick tissue samples, e.g. the embryonic whole heart, robust 3D fiber analysis tools are not available. This information is essential for computational vascular modeling and tissue microstructure characterization. Therefore, this study employs machine learning (ML) and deep learning (DL) techniques to analyze the 3D cardiovascular fiber structures in thick samples of porcine pericardium and embryonic whole hearts. It is hypothesized that ML/DL-based fiber orientation analysis will outperform traditional Fourier transform and directional filter methods by offering higher spatial accuracy and reduced dependency on manual preprocessing. We trained our ML/DL models on both synthetic and real-world cardiovascular datasets obtained from confocal imaging. The evaluation used a mixed dataset of 1147 samples and a porcine/bovine dataset of 536 samples. After applying augmentation techniques, the dataset size increased to 5649 images. Support Vector Regression (SVR) demonstrated the highest accuracy, achieving a Mean Absolute Percentage Error (MAPE) of 5.0% on the mixed dataset and 13.0% on the biological dataset. Among DL models, Convolutional Neural Network (CNN) and Residual Network-50 (ResNet50) had MAPE of 12.0% and 11.0% on the mixed dataset, and 23.0% and 22.0% on the biological dataset, respectively. Attention mechanisms improved performance further, with the Channel Attention ResNet50 achieving a MAPE of 5.8% on the mixed dataset and 21.0% on the biological dataset. These findings highlight the potential of ML and DL techniques in improving 3D fiber orientation detection, enabling detailed cardiovascular microstructural assessment.

Index Terms— Collagen, elastin, fiber orientation, machine learning, deep learning, tissue engineering, biomedical imaging, embryonic heart, pericardium

1. INTRODUCTION

Fibrous proteins, particularly collagen and elastin fibers, play a critical role in shaping the structural framework of the cardiovascular system [1]. These fibers are integral to the formation and function of cardiovascular tissues, including arteries, veins, and heart valves [2, 3]. Except the baseline endothelial membrane, cardiovascular tissues are rarely 2D and complete mapping require a 3D analysis. Understanding the orientation of collagen fibers holds particular significance in thick

cardiovascular tissues such as porcine pericardium and whole heart ventricles [4-7]. The integrity of the cardiac tissues depends on the precise alignment of its structural fibers, primarily collagen and elastin [8, 9]. Moreover, quantitative mapping of microstructural fibers is essential in cardiovascular tissue engineering, e.g. artificial surgical patches, to track changes in mechanical properties *in vivo* [10] and to optimize fiber orientation in artificial constructs [11, 12]. By ensuring accurate fiber alignment, these synthetic tissues can closely resemble the mechanical properties and functions of the biological cardiovascular tissues and enhance durability and surgical outcome.

In the literature, a myriad of 2D methods are proposed to determine the orientations of fiber structures. These include 2D Fourier transform [13, 14], Hough transform [15, 16], directional filters [17-19], intensity derivatives [20-22] or intensity variation [23], fiber tracking algorithms [24, 25], and edge detection [26]. However, 3D fiber mapping, as focused on the present paper, is limited to our knowledge. Among the 2D methods, derivative-based techniques can provide pixel-level orientation information, but they often require additional algorithms to identify the edges of the fibers across the entire image [27]. Transform or filter-based methods such as Fourier Transform or Hough Transform typically involve defining an interrogation window to obtain fiber direction within that window [28]. For fiber tracking algorithms, it is necessary to develop an algorithm that considers the spread direction of each fiber family [29]. These traditional 2D methods have several disadvantages when applied to 3D fiber analysis. First, they often lack the ability to capture the full spatial complexity and orientation of fibers in 3D. Second, these methods typically require extensive preprocessing and post-processing steps, making them less efficient and more prone to errors. Additionally, they may not generalize well to different types of tissues or varying imaging conditions.

Advances in Machine Learning (ML) and Deep Learning (DL) offer new avenues for more accurate and efficient fiber analysis, as undertaken very recently [30-34]. For instance, Zeng et al. introduced FOD-Net, a deep learning method for fiber orientation distribution angular super-resolution [30]. Nath et al. demonstrated that deep learning techniques could capture more accurate diffusion fiber orientation distributions than constrained spherical deconvolution [31]. Similarly, Karimi et al. developed a model to estimate the fiber orientation distribution function from diffusion-weighted Magnetic Resonance Imaging (MRI) [32], while Lucena et al. enhanced fiber orientation estimation using convolutional neural networks [33]. Lin et al. presented a fast-learning approach for MR tractography using a convolutional neural network [34]. However, most of these studies have concentrated on 2D data analysis or utilized clinical imaging modalities like MRI, which are suited for macroscopic tissue assessments but lack the resolution needed for 3D fiber mapping. For example, Lee et al. [35] employed ML models on multiparametric quantitative MRI data to evaluate collagen fiber orientation and proteoglycan content in articular cartilage. While impactful, these approaches reveal a gap in methods for high-resolution 3D fiber analysis. This emphasizes the need for novel techniques tailored to complex biological samples, such as those analyzed through confocal microscopy. Pham et al. present a DL model based on convolutional neural networks (CNN) for the classification and characterization of histology images. The proposed CNN model achieves over 97% accuracy in classifying normal and scar tissue, providing quantitative insights into collagen fiber density and directional variance [36]. Current studies have highlighted the potential of deep learning in cardiovascular image analysis, including heart disease detection through cardiac sounds [37] and cardiac image segmentation [38, 39].

In this study, we address this gap by introducing two novel approaches for 3D fiber orientation mapping. The proposed methods employ a robust local reconstruction technique, leveraging orthogonal 2D fiber analyses (xy and xz planes) to reconstruct comprehensive 3D fiber orientations. Additionally, the Fast Fourier Transform (FFT) algorithm is included as a benchmark to assess the comparative performance of our approaches. A significant aspect of our methodology lies in the

integration of domain-specific preprocessing steps and the exploration of advanced ML/DL techniques, including attention mechanisms such as channel attention and Convolutional Block Attention Modules (CBAM). These attention mechanisms were incorporated to enhance the analysis and evaluate their potential impact on predictive accuracy for fiber orientation mapping in thick cardiac tissues, contributing to a comprehensive comparison of methodologies. To validate our methods, we utilized a combination of synthetic datasets generated via diffusion models [40] and real-world data acquired from 3D confocal microscopy. Synthetic datasets include diverse fiber arrangements, such as toroidal structures, while real-world samples encompass thick cardiovascular tissues and embryonic heart specimens. This approach allows us to benchmark the performance of our methods across a wide range of fiber orientations and imaging conditions. This manuscript is organized as follows: First, we detail the generation of synthetic datasets and the acquisition of real-world images, followed by a comprehensive description of our methodology, including the reconstruction process and integration of ML/DL techniques. We then present a comparative analysis of our methods against the FFT benchmark, evaluating their performance in terms of accuracy, computational efficiency, and adaptability to various fiber structures. Finally, the Discussion section critically evaluates the results, highlights potential limitations, and suggests avenues for future research.

2. METHODOLOGY

The given 3D image containing fiber information was divided into smaller volumetric interrogation volumes, or voxels, to facilitate analysis. Using at least two 2D fiber direction analysis the local 3D reconstruction is achieved based on the voxel cross-sectional images along the xy- and xz- axes of the 3D image volume in Figure 1. The voxel data obtained from the xy- and xz- axes are aggregated the orientation information within each voxel, determining the resultant vector and primary orientation angle, θ , relative to a reference plane. This quantitative measure provides insight into the fiber orientation within the 3D space. To conduct this 3D analysis, we employed two new ML/DL models: Support Vector Regression (SVR) and CNN, described in Section 2.2, Section 2.3 and Section 2.4, respectively. The traditional FFT-based approach (Section 2.5), which does not involve ML/DL, is also included as a benchmark for comparisons. While FFT remains a well-established technique for frequency and orientation analysis, it primarily serves as a benchmark in this study. Existing ML/DL methods for fiber orientation mapping are limited to 2D analyses or clinical imaging modalities, such as MRI, which differ fundamentally in resolution and scope from the confocal microscopy datasets used in this research. Consequently, the methods proposed here represent a novel framework for 3D fiber orientation analysis in thick cardiac tissues, addressing challenges related to complex fiber arrangements and imaging noise.

2.1 Datasets

2.1.1 Synthetic Datasets

2D Data: In our approach to synthesizing fiber-collagen images, a diffusion model was employed to generate diverse representations. Initially, key parameters such as fiber orientation, fiber density, and structural complexity were precisely selected, forming detailed textual descriptions for the diffusion model [31]. These descriptions served as inputs to the diffusion model, guiding the generation process to produce high-resolution images with resolutions typically exceeding 1024x1024 pixels. By systematically varying these parameters, the creation of a comprehensive dataset encompassing a wide spectrum of fiber-collagen structures was ensured. This augmentation enriched our training corpus with a multitude of synthetic examples, facilitating a thorough exploration of fiber-collagen morphology. Ultimately, our approach yielded 8 high-quality synthetic

images, later cropped by 50x50 to form a total of 611 training samples, providing desired diversity to our training dataset and resulted a robust model training.

3D Data: In this study, we focused on the generation of data regarding a three-dimensional toroidal structure and its subsequent decomposition into a series of two-dimensional cross-sectional images. To achieve this, a customized algorithm was implemented, taking into consideration the geometrical properties of a torus, defined by the parametric equations [32]:

$$x(\theta, \varphi) = (R + r * \cos(\theta)) * \cos(\varphi) \quad (1)$$

$$y(\theta, \varphi) = (R + r * \cos(\theta)) * \sin(\varphi) \quad (2)$$

$$z(\theta, \varphi) = r * \sin(\theta) \quad (3)$$

The algorithm allows control over torus geometrical parameters, including its major and cross-sectional radii (R and r), as well as angular parameters (θ and φ). It generates a point cloud data of size $M \times N$, where M represents the number of torus strings and N is the number of points in each string [33]. A torus gap with an angular extent is incorporated to introduce complexity for analysis and serve as a spatial marker. Additionally, the torus can be rotated in 3D to align its normal vector with a desired plane using rotation matrices.

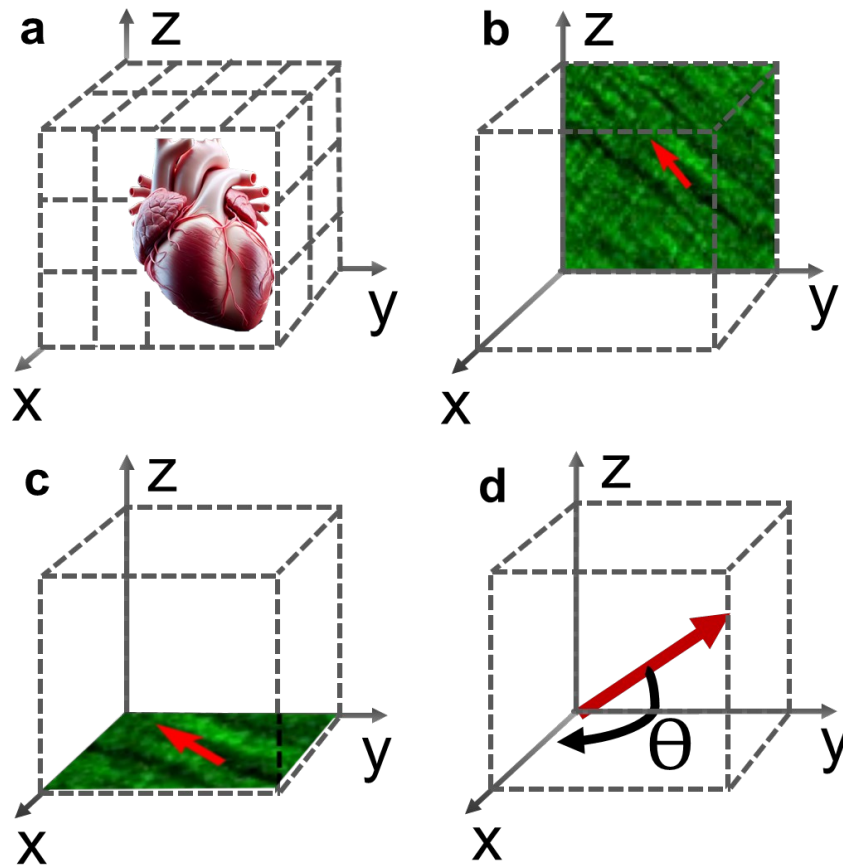


Figure 1: Cartoon representation of a thick 3D cardiovascular tissue of whole heart. (b,c) The pre-processed visualization along the xz and xy-axis using raw data. (d) 3D rendering highlighting the spatial organization of collagen fibers.

2.1.2 Biological Data

Early embryonic whole-heart samples: Fertile white Leghorn eggs are incubated according to IRB approved guidelines. Microfil agent, 2 μ L:5 μ L:5 μ L; dye: diluent buffer: curing agent, is given to the apex of the avian embryo heart *in ovo* culture (MICROFIL®Injection Compounds, Flow Tech, Inc) for vessel filling. The embryos were harvested in fresh chick ringer solution at Hamburger Hamilton (HH) stage 25 and fixed in 4% (wt/vol) paraformaldehyde [41]. This challenging dataset was specifically used as a Use Case of our ML algorithm.

Pericardium samples: Healthy porcine hearts were obtained from Koc University Hospital RMK AIMES immediately post-mortem, adhering to ethical guidelines. The pericardium was carefully dissected, rinsed with sterile saline to remove blood and debris, cut into 1 x 1 cm pieces, and fixed in 10% formalin. In addition, clinically approved porcine (BioIntegral Surgical, Inc., Canada) and bovine pericardium (Edward Lifesciences) samples were cut into 1 x 1 cm sections. These sections were permeabilized with 0.1% Triton X-100 in PBS for 2 hours, then blocked with 5% BSA in PBS for 2 hours at room temperature to prevent non-specific binding. The sections were incubated overnight at 4°C with a primary antibody against collagen I (mouse anti-collagen I) diluted 1:200 in 1% BSA in PBS. After washing with PBS, sections were incubated with Alexa Fluor® 488-conjugated anti-mouse IgG secondary antibody for 2 hours at room temperature in the dark. Stained sections were mounted on glass slides using an anti-fade mounting medium compatible with confocal microscopy.

Cardiac tissue imaging: Confocal microscopy imaging was performed using a 488 nm laser for Alexa Fluor 488. Z-stack images were acquired to capture 3D representations of collagen I distribution within both porcine pericardium and embryonic heart. Confocal microscopy were converted into 3D and visualized in xy- and xz-axes. For the algorithm, a total of 536 bovine and porcine samples were collected. This dataset was used to train and test the performance of both FFT and ML algorithms, with an 80/20 split for training and testing, respectively.

2.1.3 Training Data:

The training dataset comprises both biological and synthetic data to ensure robust model generalization. A total of 15 distinct samples were obtained from five different patches of clinically approved porcine, biological porcine and bovine pericardium, as shown in Supplementary 1. Each sample was subdivided into 50x50 voxel regions, resulting in 536 biological samples. Additionally, a diffusion model was employed to generate 8 high-resolution synthetic images, which were further divided into 50x50 voxel segments, yielding 611 synthetic samples. Collectively, the biological and synthetic data constituted a mixed dataset of 1147 samples. To improve model robustness and generalization, data augmentation techniques, including rotations, scaling, and noise addition, were applied, expanding the dataset to 5649 samples while introducing variability in fiber orientations and imaging conditions. Additionally, the training dataset was carefully balanced across different fiber orientation angles to prevent the model from overfitting to specific angles. This ensured that the model did not learn certain orientations more than others, thereby improving its ability to generalize across diverse fiber structures. Post-processing was performed on the biological images to ensure data quality by eliminating non-fiber regions, thereby retaining only relevant fiber structures. This refinement step minimized noise and ensured that the model was trained on high-quality fiber orientation data. To prevent data leakage, the synthetic images used for training were completely distinct from those used in testing. These synthetic images were designed to replicate real-world fiber structures, enhancing the model's ability to distinguish fiber orientations and adapt to complex tissue architectures.

2.1.4 Testing Data

The testing dataset was designed for both 2D and 3D verification, incorporating synthetic and biological data. For 2D validation, MATLAB-generated linear structures with controlled orientations and two separate high-quality synthetic images from diffusion models (distinct from those used in training) were included. For biological validation, a total of six samples were analyzed, obtained from three different patches (porcine and bovine), with two samples per patch, as shown in Supplementary 2. This approach ensured a comprehensive evaluation of fiber orientation variability across different anatomical sources and locations. These biological samples included clinically approved bovine and porcine pericardium as well as biological porcine pericardium, providing detailed insights into fiber orientation consistency and structural differences across tissue types. For 3D verification, the chick embryo heart dataset, containing detailed 3D fiber structure information, was used to evaluate the model's capability in reconstructing volumetric fiber orientations. No overlap existed between training and testing biological samples, ensuring unbiased evaluation.

2.2 Support Vector Regression

Histogram of gradients (HOG) feature extraction technique was utilized to capture the fine details of fiber orientations within the images. HOG is renowned for its robustness in identifying edge structures by computing the gradient orientations of localized regions within an image [42]. For each image, the method involved dividing the image into small, connected regions called grid, and for each grid, compiling a histogram of gradient directions or edge orientations. By normalizing these histograms across larger regions of the image, invariance to the changes in illumination and shadowing was achieved. To determine the optimal grid size for feature extraction, various grid sizes such as 4x4, 8x8, 16x16, and 32x32 were tested. After extensive testing, it was found that the 32x32 grid size provided the best balance between detailed feature capture and computational efficiency for our image size 1024 x 1024. However, to avoid missing small details with the large grid size, all features from 4x4, 8x8, 16x16, and 32x32 were used. This configuration resulted in a comprehensive feature set that effectively characterizes the patterns and structures underlying fiber-collagen arrangements, providing a solid foundation for subsequent ML tasks.

Following feature extraction, SVR technique was employed to train the regression model. SVR is particularly adept at handling high-dimensional feature spaces and is capable of learning complex mappings between input features and target values. As illustrated in Figure 2, the SVR model was trained to predict the actual fiber orientation angles from the extracted HOG features. By utilizing a kernel function, the non-linear relationships within the data were managed, enhancing predictive accuracy. A grid search was conducted to find the optimal hyperparameters for the SVR model, considering different kernel types, i.e. linear and radial basis function (rbf), regularization parameters (C), and kernel coefficients (gamma). This optimization approach, facilitated by cross-validation techniques, ensured robustness and generalization of performance, making the SVR model a reliable tool for analyzing and predicting fiber orientations even in test data.

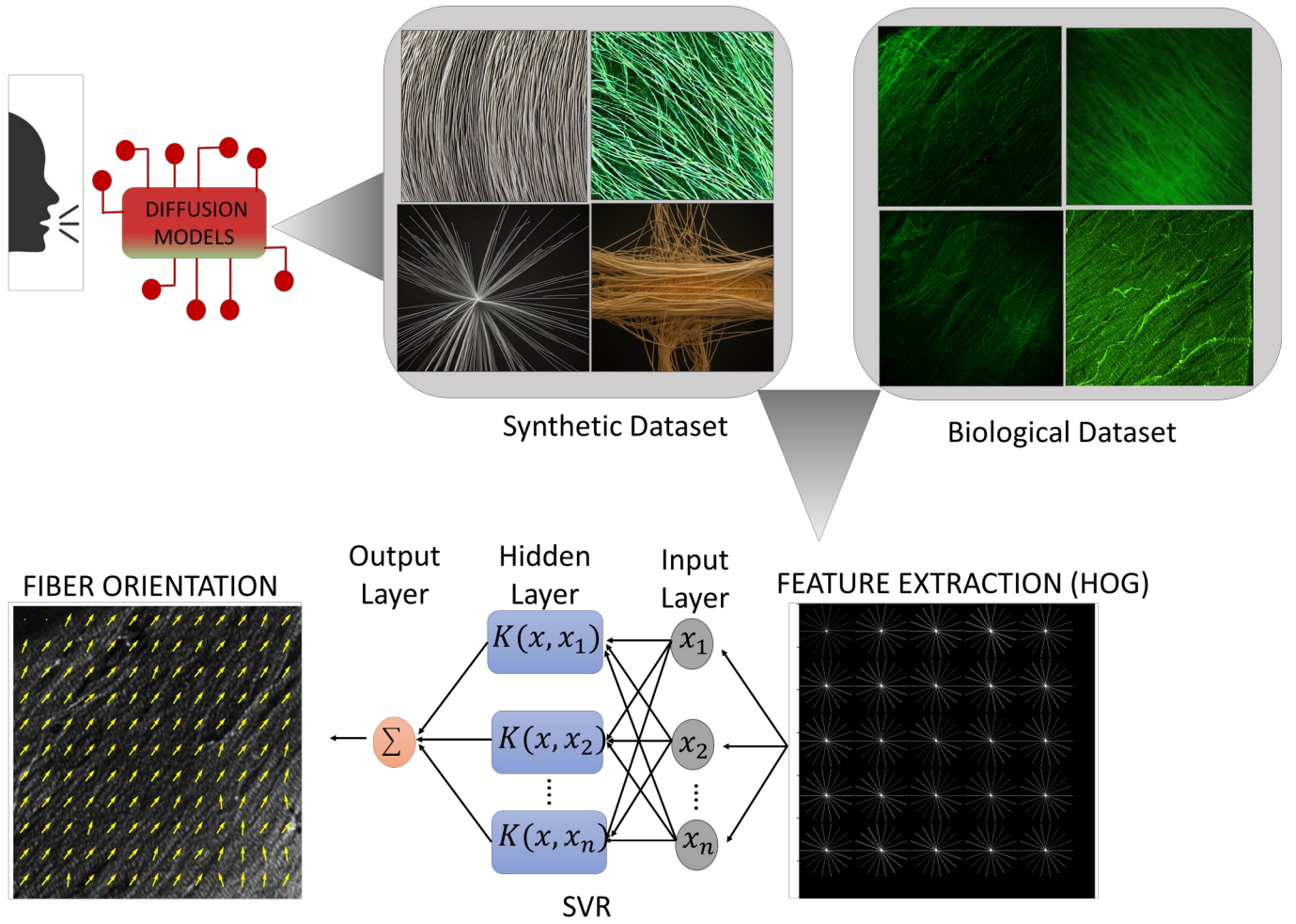


Figure 2: Process of estimating fiber orientation using both synthetic and biological datasets. Synthetic images are generated through diffusion models, creating diverse fiber patterns, which are then compared with actual biological fiber images captured via microscopy. Feature extraction is performed on both datasets using HOG, emphasizing the directionality and distribution of fiber orientations. These features are subsequently input into a SVR model, where the input layer consists of feature vectors processed through kernel functions in the hidden layer. The output layer sums these contributions to predict fiber orientation. The analysis culminates in detailed orientation maps, exemplified by yellow arrows on a sample image, providing comprehensive insights into the structural organization of fibers in synthetic and biological samples.

2.3 Convolutional Neural Network Training

In the deep learning phase, a CNN was utilized to analyze and discern complex spatial relationships within the fiber orientation data. CNNs are particularly well-suited for fiber image analysis task due to their ability to learn hierarchical representations of data through layers of convolutional filters [43]. Our CNN architecture included two convolutional layers, each followed by activation functions and pooling layers, which contributed to robust feature extraction and representation. Specifically, the model consisted of an input layer for 50x50 grayscale images, multiple convolutional layers with ReLU activation and max-pooling, followed by dense layers with dropout for regularization. We applied data augmentation techniques like random rotation, translation, and horizontal flipping to enhance the model's generalization. The model was trained with the Adam optimizer for 200 epochs and Mean Absolute Error (MAE) was used as a loss function.

2.3.1 Transfer Learning

To further enhance the performance and efficiency of DL models, transfer learning was leveraged, incorporating pre-trained CNN models from well-established architectures such as ResNet50 [44]. Transfer learning involved using models that had been pre-trained on large image datasets, such as ImageNet, which contains millions of images across thousands of categories. Fine-tuning the pre-trained model involved selectively unfreezing and retraining specific layers, allowing the model's learned representations to adapt to the nuances of the fiber orientation dataset. This approach allowed for accelerated convergence, as the models required fewer epochs to adapt to the dataset.

2.3.2 Attention Mechanisms

To enhance the model's ability to focus on the most relevant regions and features of the images, attention mechanisms are incorporated into the architecture [45]:

Channel Attention: This mechanism emphasizes critical feature channels by calculating a learnable scaling factor through global average pooling and dense layers. It effectively highlights channel-specific information crucial for accurate predictions.

Spatial Attention: Spatial attention highlights significant spatial regions within the feature maps. By aggregating pooled feature maps (max and average) and passing them through a convolutional layer, the model dynamically focuses on regions relevant to fiber orientation.

2.4 Fast Fourier Transform (Benchmark)

Fiber orientation can be obtained based on the variability of voxel intensities in all directions within a 3D image stack using the 3D FFT [49]. In our approach, we divide a slice into typically 50x50 grids, resulting in smaller-sized images. Subsequently, a 2D FFT is applied to each of these smaller images. The vectors are then obtained using the 3D analysis method.

In the analysis of biological data, artifacts present in images can lead to the emergence of "bad" fiber directions (vectors) disrupting the accuracy of angle estimation in FFT analysis. To address this issue, we initially applied FFT to the entire image to obtain the frequency spectrum and identified the angle corresponding to the maximum amplitude. Vectors deviating within a range of 0-20 degrees from this dominant angle were classified as bad vectors. These vectors were removed, and the image was adjusted to align with the most dominant angle present.

2.5 Performance Evaluation

The primary performance metric for evaluating our regression models was the Mean Absolute Percentage Error (MAPE). MAPE offers a clear and intuitive measure of the average magnitude of errors between the predicted and actual fiber orientation angles, expressed as a percentage. It is calculated as the average of the absolute percentage differences between predicted values and the ground truth values, providing a straightforward assessment of prediction accuracy. Specifically, MAPE is defined by the formula:

$$MAPE = \frac{1}{n} \sum_{i=1}^n \left| \frac{y_i - \hat{y}_i}{y_i} \right| \times 100$$

where y_i represents the actual fiber orientation angle, \hat{y}_i is the predicted angle, and n is the total number of predictions. Using MAPE as our primary performance metric allowed the overall accuracy of our both FFT and ML models in predicting fine-

grained fiber orientations. Lower MAPE values indicate better model performance, reflecting more precise and accurate predictions. By systematically analyzing the MAPE of our models, we could identify specific areas where our models excelled and where further improvements were necessary. This metric was instrumental in guiding the iterative refinement of our models, ensuring that we progressively enhanced their predictive capabilities and robustness.

3. RESULT

3.1 3D FFT Approach (Benchmark)

We create benchmark results using our FFT method with two different datasets: synthetically generated data and bovine/porcine data. The determination of angles for diverse linear structures was accomplished using a 2D FFT technique, enabling the analysis of signal components along various directions. For the synthetic dataset, lines were generated using a script and positioned at 45, 60, and 135 degrees, as illustrated in Figure 3. The analysis revealed a slight 2-degree deviation from the anticipated 180-degree angle, suggesting that the method effectively discerns the angles formed by the linear structures with respect to the x-axis, achieving a notable accuracy rate of 98.9%.

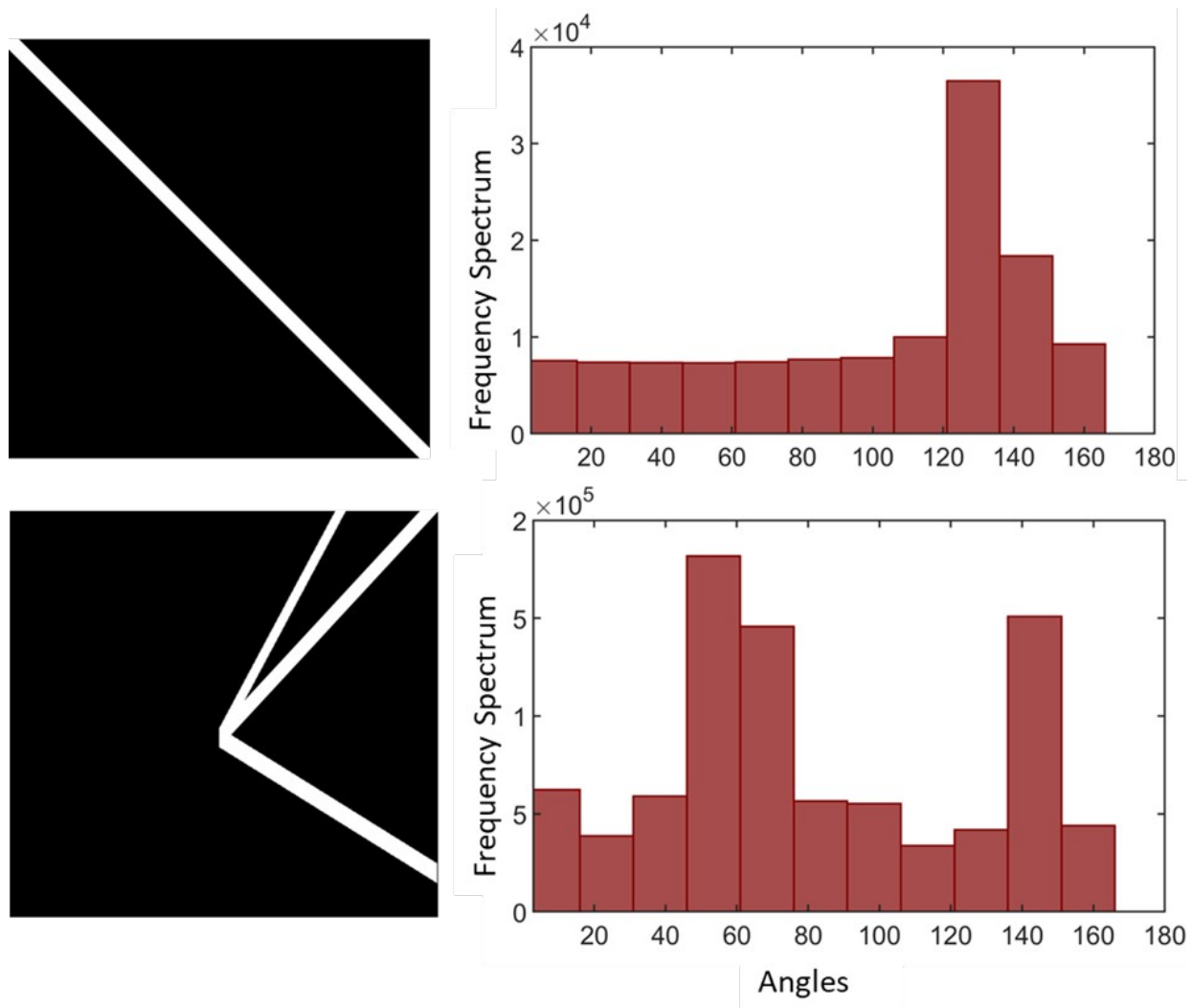


Figure 3: FFT Analysis for 2D Synthetic Data. (a-d) Lines with 45, 60 and 135 degree angles are produced as binary scale using MATLAB, and the graph of the analysis results is shown using 2D FFT and x axes represent to angle of line, y axis represent to frequency spectrum.

The orientations of fiber structures in clinically approved and biological porcine slices were similarly analyzed using 2D FFT, as depicted in Figure 4. For clinically approved bovine samples, a dominant fiber orientation at 130 degrees was recorded, with a deviation of 3.8% in Figure 5. In contrast, clinically approved Porcine samples exhibited a dominant orientation at 140 degrees, with a deviation of 11.1%, indicating a 7.3% increase compared to clinically approved bovine. biological porcine showed a dominant fiber orientation at 135 degrees, with a deviation rate of 8.3%. These angles are measured with respect to the apicobasal direction of the heart.

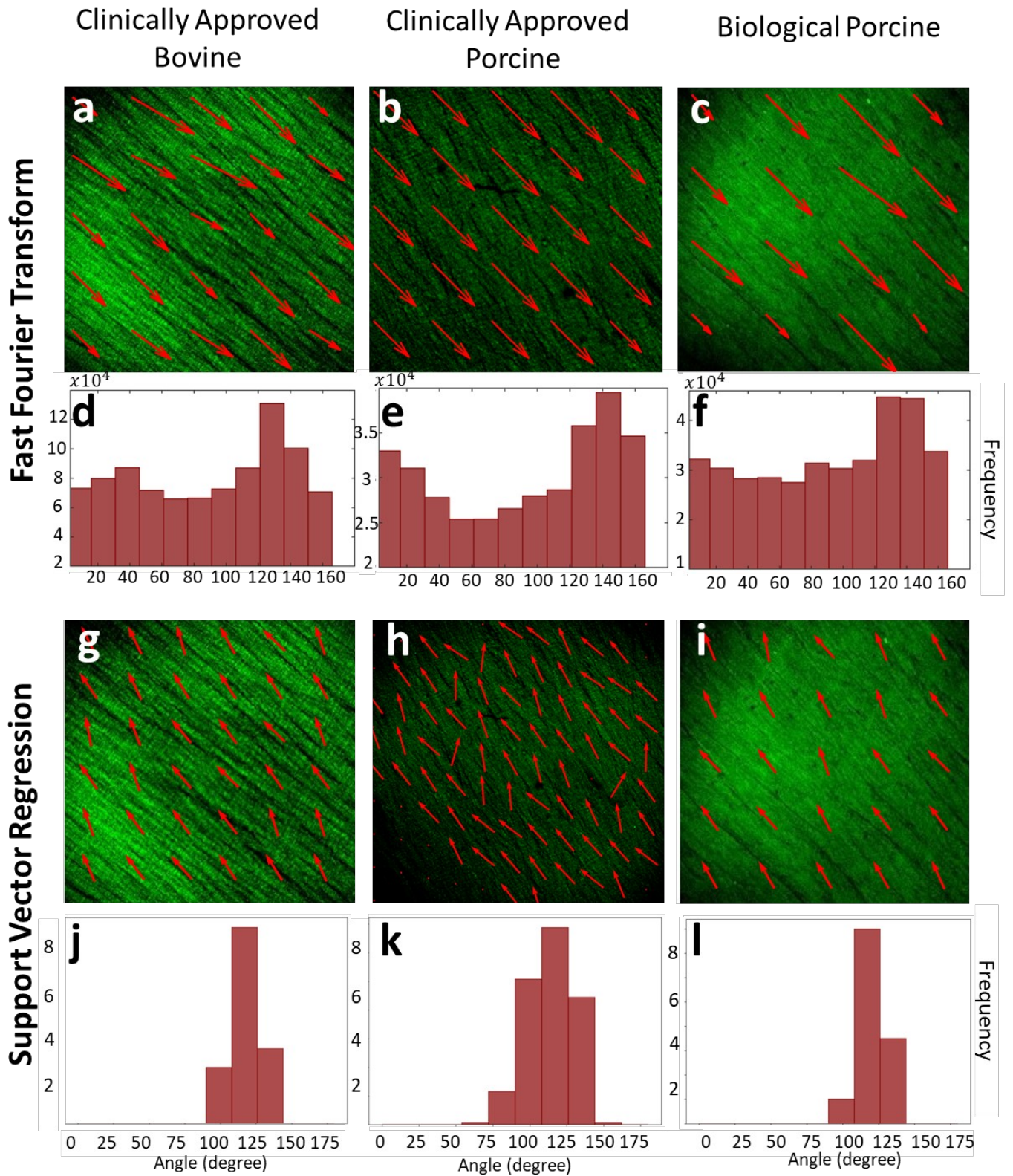


Figure 4: Comparison of fiber orientation estimation in different tissue samples using FFT and SVR. The top row (a-c) shows fiber orientation maps (red arrows) overlaid on green fluorescence images for clinically approved bovine (a), clinically approved porcine (b), and biological porcine (c) tissues analyzed using FFT. The corresponding histograms (d-f) depict the distribution of fiber angles obtained from FFT analysis, with angles ranging from 20 to 160 degrees. The bottom row (g-i) displays fiber orientation maps (red arrows) for the same tissue samples analyzed using SVR. The associated histograms (j-l) show the distribution of fiber angles derived from SVR analysis, with

angles concentrated around 100 degrees. This comparison highlights the differences in fiber orientation results between FFT and SVR methods across different tissue types.

To further explore potential statistical differences among clinically approved bovine, clinically approved porcine, and biological porcine samples, an ANOVA test was conducted. The results suggested that there was no statistically significant variation in the dominant fiber orientations among the three groups.

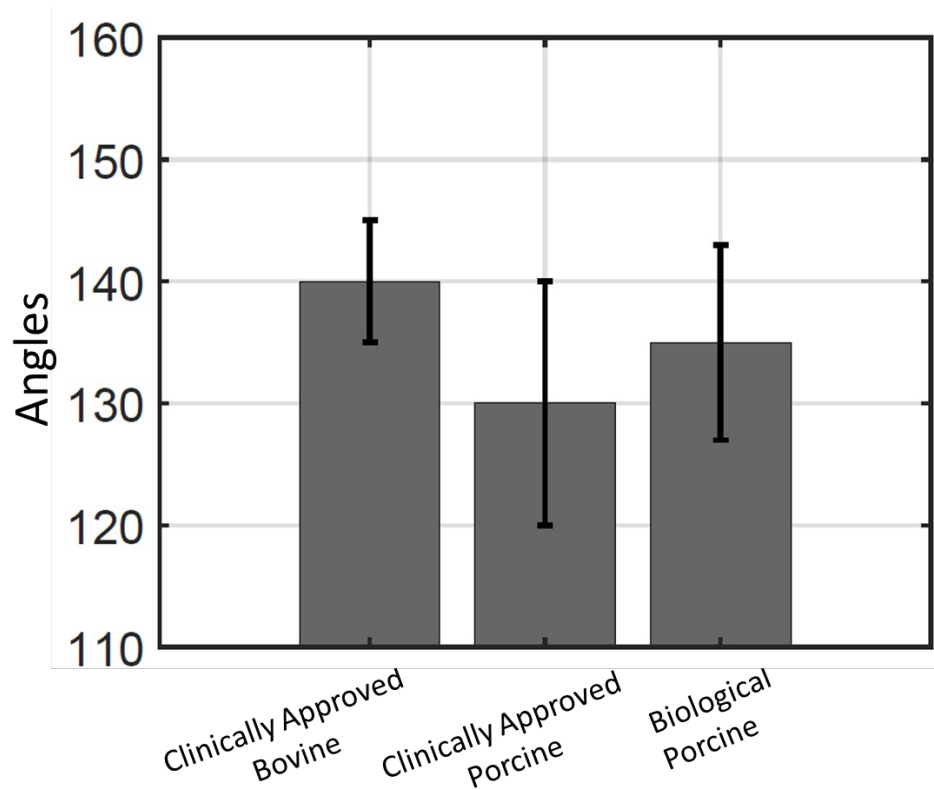


Figure 5: Analysis of Fiber Orientation via 2D FFT for clinically approved bovine, clinically approved porcine, and biological porcine samples. sixth samples were analyzed for each case, illustrating the mean angle of fiber orientation accompanied by standard deviation lines. These sixth samples consist of two samples from third different pericardia, with two different locations each, providing comprehensive insights into fiber orientation variability across different anatomical sources and locations

3.2 Validation of the 3D Representation

We validated the 3D vector integration method using FFT with a synthetic dataset. The 3D FFT method was applied to datasets of three-dimensional helical and toroidal structures to determine vector orientations. For the helical structure, the dataset with dimensions of 900x900x900 pixels was divided into 30x30x30 pixel grids, generating a total of 30x30x30 vector maps. Similarly, the toroidal structure, with the same dimensions, was processed to create 30x30x30 vector maps. Each vector was mapped to the nearest point on the respective structures and interpolated to ensure continuity. The method demonstrated a mean accuracy of 97% for the helix and 91.8% for the torus, as shown in Figures 6a and 6b.

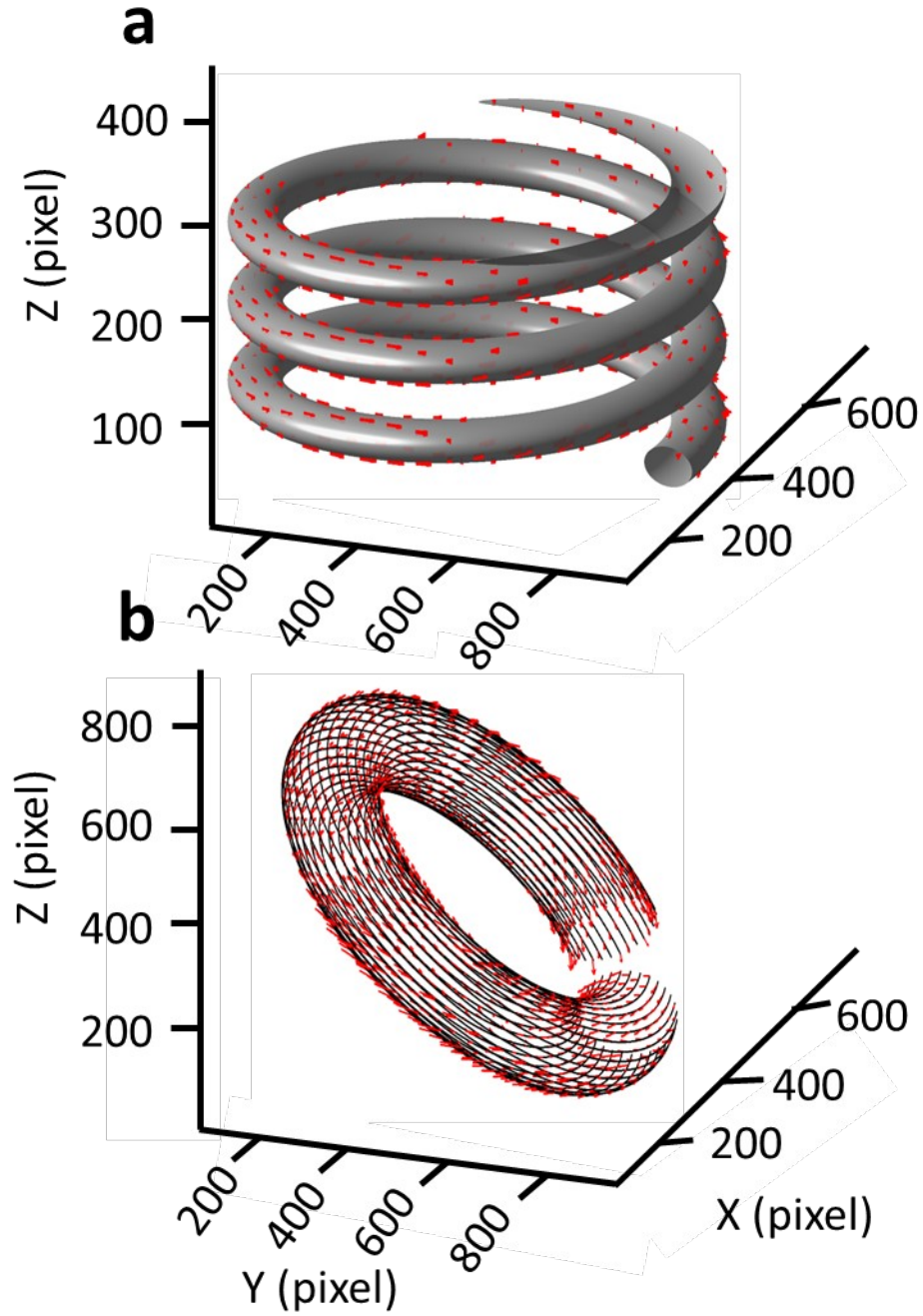


Figure 6: 3D Synthetic Torus Analysis Using 3D FFT. (a, b) Combined visualization showing the 3D structure of the helix and torus with detailed fiber orientation analysis using 3D FFT.

3.3 Performance of MLIDL Models

In our study, we employed both SVR, CNN, ResNet50 with attention mechanism to analyze the orientation of collagen fibers in various tissue samples.

In Table 1, SVR emerged as the most accurate Machine Learning model, achieving a MAPE of 5.5% on the mixed dataset, which corresponds to an average error of 10 degrees. This indicates that SVR can predict fiber orientation with a high degree of accuracy. However, its performance on the biological dataset was lower, with a MAPE of 13%.

Table1: Performance comparison of different models used in our analysis across the mixed and biological datasets. The values represent the error rates (\pm standard deviation). SVR denotes Support Vector Regression, CNN represents Convolutional Neural Network, ResNet50 refers to Residual Neural Network, CBAM Attention CNN indicates the Convolutional Block Attention Module applied to CNN, and Channel Attention ResNet50 represents ResNet50 integrated with a channel attention mechanism.

Algorithms	Mixed Dataset	Biological Dataset
<i>SVR [42]</i>	5 ± 0.2	13 ± 0.7
<i>CNN [43]</i>	12 ± 3.7	23 ± 2
<i>ResNet [43]</i>	11 ± 0.4	22 ± 1.1
<i>CBAM Attention [45] CNN</i>	11 ± 0.6	18 ± 0.9
<i>Channel Attention ResNet</i>	5.8 ± 0.4	21 ± 1

Among the deep learning models, the CNN yielded a MAPE of $12 \pm 3.7\%$ on the mixed dataset, corresponding to an average error of approximately 21 degrees, and $23 \pm 2\%$ on the biological dataset, with potential for improvement through parameter tuning and augmentation. ResNet50 performed slightly better, achieving a MAPE of $11 \pm 0.4\%$ on the mixed dataset and $22 \pm 1.1\%$ on the biological dataset. Incorporating attention mechanisms further enhanced the models' performance. The CBAM Attention CNN achieved a MAPE of $11 \pm 0.6\%$ on the mixed dataset and $18 \pm 0.9\%$ on the biological dataset, while the Channel Attention ResNet50 achieved the best performance among the deep learning models, with a MAPE of $5.8 \pm 0.4\%$ on the mixed dataset and $21 \pm 1\%$ on the biological dataset, highlighting the effectiveness of attention mechanisms in improving prediction accuracy. Compared to these, the SVR model demonstrated robust performance, achieving a MAPE of $5 \pm 0.2\%$ on the mixed dataset and $13 \pm 0.7\%$ on the biological dataset, making it the most accurate approach for further analysis.

3.4 Test of SVR model with real data

Finally, we validated the SVR method using two different datasets: synthetically generated data and bovine/porcine collagen data. To demonstrate the reliability of our model, we first analyzed synthetic collagen fiber structures generated by the diffusion model, using SVR to determine fiber orientations. Figures 7a and 7d depict the overall fiber structures, with red arrows indicating

the orientations predicted by SVR. Detailed views in Figures 7b and 7e focus on the specific fiber orientations within the yellow-highlighted areas of Figures 7a and 7d, respectively. The angle distribution histograms in Figures 7c and 7f quantify the orientation angles of the fibers. In Figure 7c, the histogram reveals distinct peaks around 25° and 125° , indicating a strong preferential alignment of fibers at these angles in the synthetic model. Conversely, the histogram in Figure 7f exhibits a more uniform distribution of fiber angles, reflecting the diverse and complex orientations in the synthetic dataset generated by the diffusion model. The circular structure of the image contributes to this uniform distribution of angles from 0° to 180° .

To further assess the accuracy of our models, we analyzed 2D collagen images from various sources. Figure 4 presents the results for nine images. The clinically approved bovine collagen sample displayed a predicted orientation marked by a red arrow, along with the corresponding angle distribution histogram.

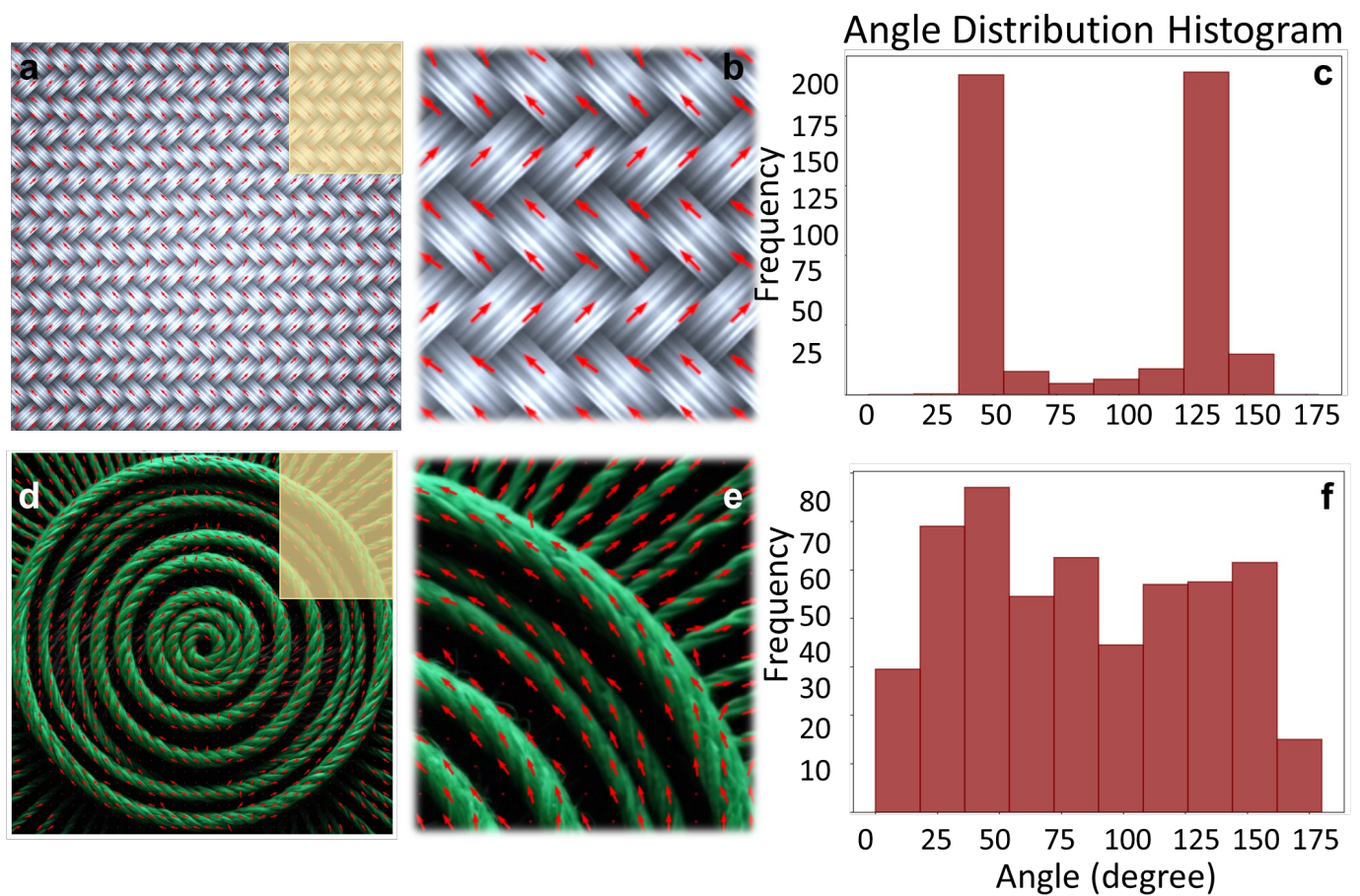


Figure 7: Visual representation and angle distribution of collagen fiber orientation. (a) and (d) show the collagen fiber structures obtained from the diffusion model. (b) and (e) are magnified views of the yellow highlighted areas in (a) and (d), respectively, providing a detailed view of fiber orientation within those regions. (c) and (f) are angle distribution histograms corresponding to the fiber structures shown in (a) and (d), respectively.

Figure 4j illustrates a predominant orientation of approximately 120 degrees, with variations ranging between 100 and 140 degrees. The clinically approved porcine collagen sample shown in Figure 4h exhibited predicted orientations at 100 and 120 degrees, highlighted by the red arrow, while the angle distribution histogram in Figure 4k displayed variations between 90 and

130 degrees. The biological porcine collagen sample presented in Figure 4i showed a predominant orientation around 120 degrees, also indicated by the red arrow, with its angle distribution histogram in Figure 4l revealing variations between 100 and 140 degrees. These findings confirm the robustness and reliability of our models in accurately predicting collagen fiber orientations across different tissue types.

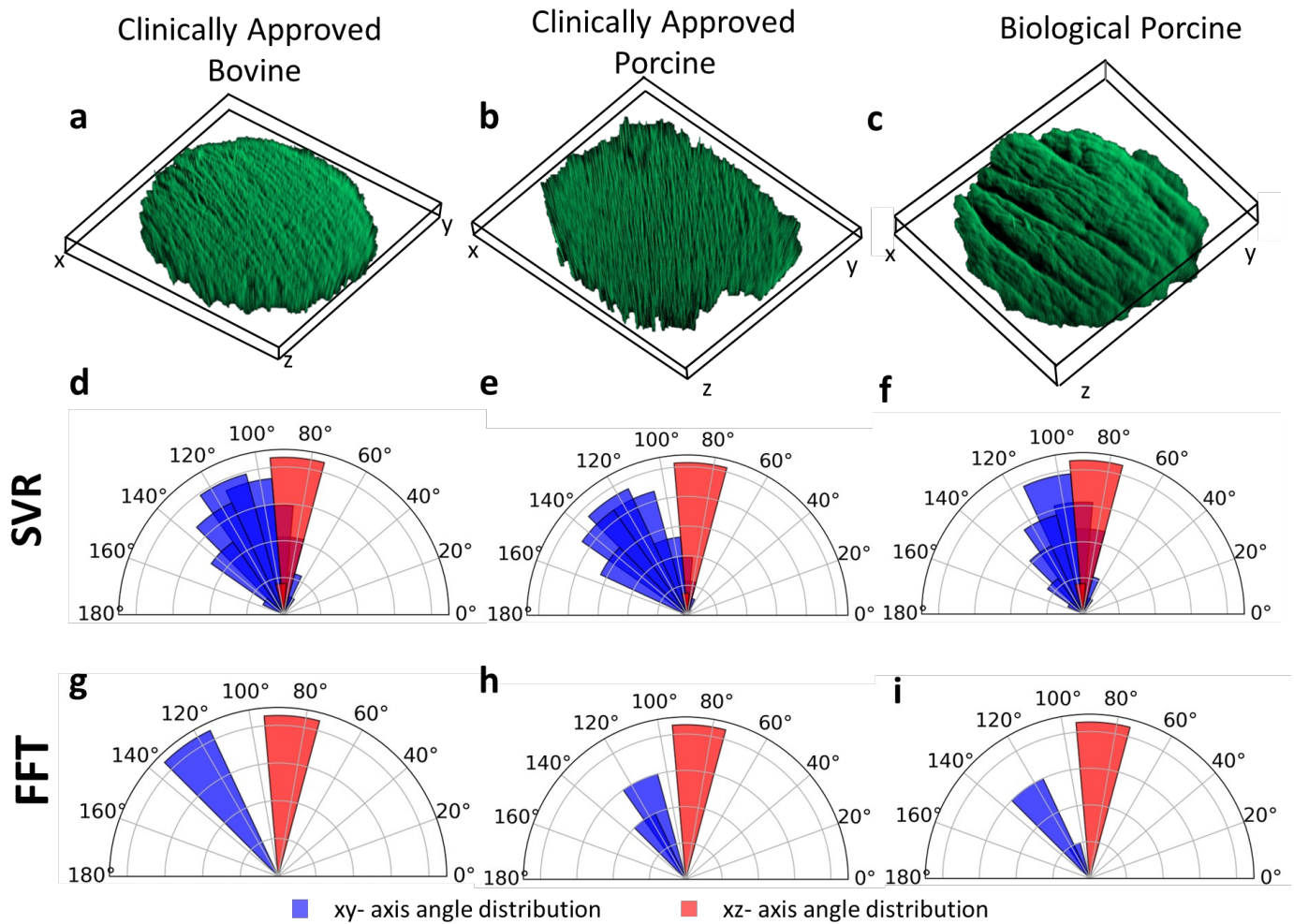


Figure 8: 3D visualization and orientation analysis of fiber structures in clinically approved bovine, clinically approved porcine, and biological porcine tissues. a-c show 3D reconstructions of confocal microscopy slices, processed and visualized using Huygens, for clinically approved bovine (a), clinically approved porcine (b), and biological porcine (c) samples. d-f display the angular distribution of fiber orientations along the xy-axis (blue) and xz-axis (red), obtained through Fourier transform analysis in MATLAB. g-i provide the angular distribution of fiber orientations obtained from Support Vector Regression.

We extended our analysis to 3D collagen fiber orientation in porcine and bovine samples, leveraging advanced imaging and modeling techniques. Figure 8 presents the comprehensive results of this analysis. Figures 8a through 8c show 3D visualizations of collagen fiber orientations for clinically approved bovine, clinically approved porcine, and biological porcine samples, respectively. Figures 8d through 8f display the polar distribution visualizations obtained using SVR, while Figures 8g through 8i depict the results derived from FFT. For clinically approved bovine samples, the SVR results in Figure 8d indicate predominant fiber orientations around 120 degrees along the xy-axis and 90 degrees along the xz-axis, whereas the FFT results in Figure 8g

show predominant orientations at 130 degrees along the xy-axis and 90 degrees along the xz-axis. In clinically approved porcine samples, the SVR results in Figure 8e reveal predominant fiber orientations at 120 and 130 degrees along the xy-axis and 90 degrees along the xz-axis, while the FFT results in Figure 8h confirm a predominant orientation at 120 degrees along the xy-axis and 90 degrees along the xz-axis. For biological porcine samples, the SVR results in Figure 8f indicate predominant fiber orientations at 120 and 110 degrees, with some variation around 120 degrees along the xy-axis, and a consistent orientation around 90 degrees along the xz-axis. The FFT results in Figure 8i similarly show predominant fiber orientations at 130 degrees along the xy-axis and 90 degrees along the xz-axis. These results demonstrate that our models effectively capture the complex 3D orientations of collagen fibers in porcine and bovine samples, showcasing their robustness and accuracy. This capability enhances our understanding of the structural organization in biological tissues, with significant implications for developmental biology and tissue engineering, where precise knowledge of fiber orientation is critical.

To further evaluate our approach, we applied it to predict the 3D collagen fiber orientation in early chick embryo heart samples as a challenging use case. Figure 9 provides the comprehensive results of this analysis. Figure 9a presents a 3D vector field visualization of collagen fibers in the chick embryo sample, with red arrows indicating the predicted orientations. Figure 9b shows a confocal microscopy image that details the structural organization of the collagen fibers throughout the ventricle. The polar distribution visualization in Figure 9c indicates a predominant fiber orientation around 90 degrees. Figure 9d offers a volumetric rendering of the sample, highlighting the spatial distribution and organization of the collagen fibers. Additionally, a 3D vector field visualization in Figure 9e illustrates regions with varied fiber orientations, which are confirmed by the corresponding confocal microscopy image in Figure 9f. The polar distribution visualization in Figure 9g reveals predominant orientations around 45 and 90 degrees for the region shown in Figure 9e along the xy-axis, while the xz-axis consistently shows a predominant orientation at 90 degrees. These findings underscore our model's effectiveness in capturing complex 3D fiber orientations, facilitating a deeper understanding of structural organization in biological tissues. This work has significant implications for developmental biology and tissue engineering, particularly in advancing our knowledge of collagen fiber arrangement and its functional roles.

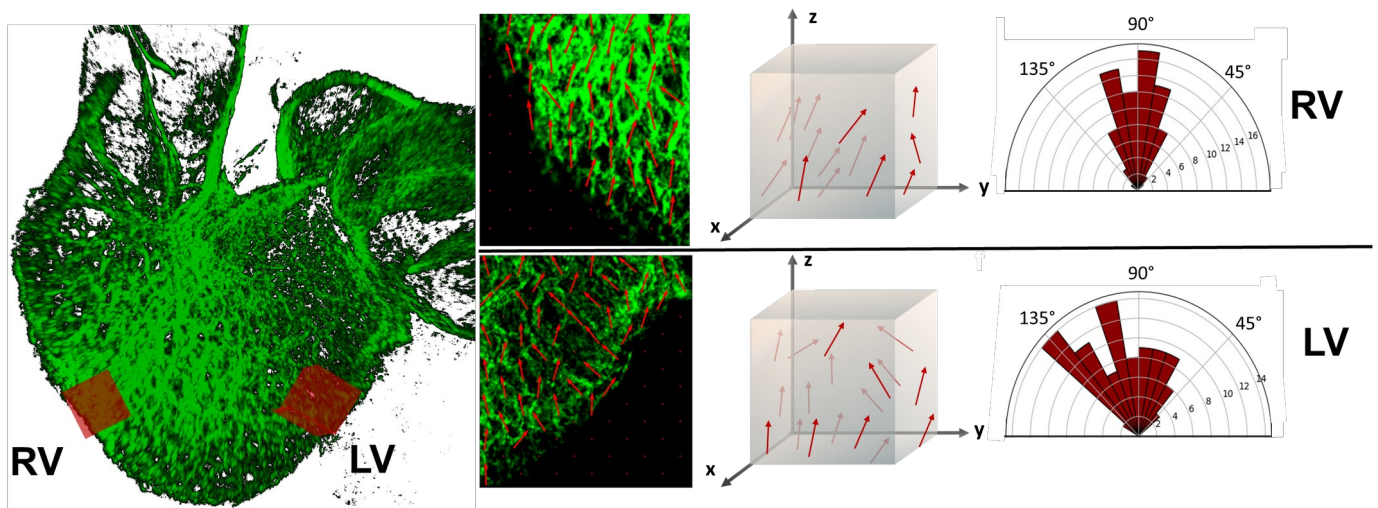


Figure 9: Comprehensive analysis of 3D collagen fiber orientation in chick embryo heart samples using advanced imaging and modeling techniques. The first row focuses on the right ventricle (RV), showing a 3D rendering of the heart (first column), a high-resolution 2D confocal microscopy image of collagen fibers (second column), a 3D vector field visualization of fiber orientations (third column), and a polar

distribution plot illustrating predominant fiber orientation around 90 degrees (fourth column). The second row provides similar analyses for the left ventricle (LV), with corresponding visualizations and orientation data.

4. DISCUSSION

4.1 Synthetic Data Generation and Utilization

Due to the inherent nature of biological data, which tend to have different fiber families concentrated at specific angles, model training naturally introduced biases, prioritizing these angles [46]. To address this issue, we generated synthetic data using a diffusion model and subsequently trained our models with this data. The synthetic dataset provided a controlled environment to ensure that the models were not biased towards a particular orientation. This was achieved by generating fibers at various angles. It was crucial to provide the diffusion models with accurate descriptions to obtain the required images. Therefore, the detailed description and quality of the dataset played a significant role in training robust models capable of generalizing to real-world application.

4.2 Feature Extraction Approaches

Models trained with features extracted from images using HOG are significantly affected by the grid size [47]. The grid size determines the structure of the feature map by affecting the granularity and scale of the captured features. A finer grid size results in more detailed feature extraction by capturing subtle variations in the image, which can be crucial for accurately modelling complex patterns such as collagen fiber orientations. Conversely, a coarser grid size can miss these details but reduces computational complexity and noise. Therefore, choosing the appropriate grid size is crucial and needs to be tailored the images being analyzed, with this study utilizing a grid size of 32x32. Moreover, the HOG parameters should be adapted to the specific characteristics of the dataset, such as the image resolution and the scale of the analyzed structures. This adaptability contributes to the overall effectiveness of the model by ensuring that the extracted features are both relevant and robust.

4.3 Comparative Model Performance

In this study, we employed both ML and DL techniques, including SVR, CNN, ResNet50, and attention-based DL models. Among these approaches, SVR demonstrated the most effective performance, excelling in terms of accuracy and computational efficiency. Its success can be attributed to its ability to handle high-dimensional feature spaces effectively while avoiding overfitting, particularly when applied to well-structured synthetic datasets. While DL models such as CNN and ResNet50 achieved competitive results, they did not surpass the performance of SVR in this context. This highlights that simpler, more interpretable machine learning techniques can sometimes outperform complex DL models for tasks where the feature space is well understood and relatively structured, such as fiber orientation analysis.

The DL models showed significant potential due to their advanced feature extraction capabilities but required extensive tuning, larger datasets, and advanced techniques like data augmentation and transfer learning to realize their full potential. The inclusion of attention mechanisms, for example, enhanced their performance, demonstrating the importance of architectural advancements in improving accuracy. However, the superior efficiency and robustness of SVR underline the critical need for algorithm selection based on the nature of the data and the specific requirements of the task.

Additionally, a comparison with FFT, used as a benchmark method, revealed notable advantages of SVR. While FFT is a reliable and well-established approach for analyzing frequency and orientation, it requires multiple preprocessing and post-processing steps for accurate results. In contrast, SVR simplifies the workflow by eliminating the need for these additional steps while achieving faster processing times. This efficiency, coupled with its strong performance, makes SVR a practical choice for applications involving large datasets and real-time analysis. These findings reinforce the importance of balancing model complexity, performance, and interpretability in the development of biomedical image analysis tools and other computational methods.

4.4 Fiber Orientation across Porcine Tissues

The ANOVA results indicated no statistically significant differences in the dominant fiber orientations among clinically approved bovine, clinically approved porcine, and biological porcine tissues in FFT analyses. This finding suggests that these tissue types share a similar primary fiber alignment. Given this similarity, clinically approved bovine and porcine tissues may be considered interchangeable in applications where fiber orientation is a key structural parameter. Particularly in tissue engineering and biomedical applications, this consistency supports the use of porcine pericardium as a scaffold or decellularized matrix, offering a practical and scalable option. In cases where biological porcine tissue availability is limited, clinically approved alternatives may provide viable substitutes.

Additionally, 3D FFT analyses helped reveal the broader architectural organization of these tissues, confirming that the primary fiber alignment remains unchanged regardless of tissue type. This structural consistency could be valuable for designing engineered constructs that replicate the mechanical properties of native tissues. From a clinical perspective, understanding fiber orientation is essential for optimizing surgical patch designs and improving tissue-engineered heart valves. The ML/DL-based approach presented in this study provides a more refined method for analyzing fiber alignment, which could aid in the development of personalized cardiovascular implants and regenerative therapies. Furthermore, high-resolution fiber mapping may enhance computational models used in surgical planning and disease diagnostics, particularly in conditions affecting collagen organization.

5. CONCLUSION

This study compared the effectiveness of traditional FFT with advanced ML and DL models for analyzing collagen fiber orientations in various tissue samples. The findings emphasized the strengths and limitations of each approach, demonstrating the advantages of ML and DL models over the traditional FFT method in handling complex scenarios. While FFT remains effective for basic 2D and 3D fiber orientation analyses, it encounters challenges in processing noise and structural variations present in complex tissue architectures. Although FFT performed well in synthetic and biological datasets, its applicability diminishes as tissue complexity increases due to its reliance on extensive preprocessing and assumptions about uniformity.

In contrast, ML and DL models, including SVR, CNN, ResNet50, and attention-enhanced architectures, exhibited superior robustness and accuracy in analyzing intricate fiber patterns. These models excelled in their ability to learn from diverse datasets, adapting to variations in tissue structures and reducing the impact of noise. Among them, SVR consistently provided precise and interpretable results, highlighting its efficiency in characterizing fiber orientations. DL models further demonstrated their potential for deeper tissue analysis, especially with advanced techniques like transfer learning and attention mechanisms, which improve performance in challenging cases.

In conclusion, while FFT serves as a reliable tool for basic analyses, ML and DL models significantly advance the field by offering improved accuracy, automation, and adaptability to complex biological structures. These methods deepen our understanding of tissue architecture and hold promise for applications in biomedical research, tissue engineering, and computational modeling. Future efforts should focus on refining these models further, exploring novel architectures, and extending their use to other intricate biological systems.

Acknowledgements:

We would like to acknowledge the support from the European Research Council (ERC) Proof of Concept *BloodTurbine* 966765, TUBITAK 118S108 and BİDEB - 2247A - 120C139 also BİDEB 2211A.

Disclosures. The authors declare no conflicts of interest.

Data availability

The data underlying the results presented in this paper are available in the [GitHub](#) repository. The dataset is structured into training and testing datasets as follows:

Training Dataset

- Biological Data: 15 different sample from 5th different patch (Clinically approved bovine and porcine, biological porcine) images.
- Synthetic Data: 8 high-quality synthetic images generated using diffusion models, further divided into 50×50 voxel segments.
- Augmented Data: 5649 images

Testing Dataset

- Chick Embryo: Heart slice scans in 2D.
- Clinically Approved Bovine: Nine patches, with three having 3D slice scans.
- Clinically Approved Porcine: Seven patches, with four having 3D slice scans.

- Biological Porcine: Seven patches, with one having 3D slice scans.
- Synthetic Data: 2 different synthetic data generated by diffusion models, 2 different data generated by MATLAB.

The data can be accessed via the link above.

Code Availability

The code used in this study is publicly available at the [GitHub](#) repository. This repository contains all necessary scripts, model implementations, and dataset processing pipelines used for fiber orientation mapping.

REFERENCES

1. Balasubramanian, P., et al., *Collagen in Human Tissues: Structure, Function, and Biomedical Implications from a Tissue Engineering Perspective*. Fortschritte der Hochpolymeren-Forschung, 2013. **251**: p. 173.
2. Schoen, F., *Evolving Concepts of Cardiac Valve Dynamics The Continuum of Development, Functional Structure, Pathobiology, and Tissue Engineering*. Circulation, 2008. **118**: p. 1864-80.
3. Sarraf, C.E., et al., *Heart valve and arterial tissue engineering*. Cell Prolif, 2003. **36**(5): p. 241-54.
4. Gasser, T.C., R.W. Ogden, and G.A. Holzapfel, *Hyperelastic modelling of arterial layers with distributed collagen fibre orientations*. J R Soc Interface, 2006. **3**(6): p. 15-35.
5. Capulli, A.K., et al., *Fibrous scaffolds for building hearts and heart parts*. Adv Drug Deliv Rev, 2016. **96**: p. 83-102.
6. Carruthers, C.A., et al., *GENE EXPRESSION AND COLLAGEN FIBER MICROMECHANICAL INTERACTIONS OF THE SEMILUNAR HEART VALVE INTERSTITIAL CELL*. Cell Mol Bioeng, 2012. **5**(3): p. 254-265.
7. Sulejmani, F., et al., *Evaluation of transcatheter heart valve biomaterials: Computational modeling using bovine and porcine pericardium*. J Mech Behav Biomed Mater, 2019. **97**: p. 159-170.
8. Robinson, T.F., et al., *Structure and function of connective tissue in cardiac muscle: collagen types I and III in endomysial struts and pericellular fibers*. Scanning Microsc, 1988. **2**(2): p. 1005-15.
9. Kitsara, M., et al., *Fibers for hearts: A critical review on electrospinning for cardiac tissue engineering*. Acta Biomater, 2017. **48**: p. 20-40.
10. Simionescu, D.T., et al., *Form Follows Function: Advances in Trilayered Structure Replication for Aortic Heart Valve Tissue Engineering*. J Healthc Eng, 2012. **3**(2): p. 179-202.
11. Sellaro, T.L., et al., *Effects of collagen fiber orientation on the response of biologically derived soft tissue biomaterials to cyclic loading*. J Biomed Mater Res A, 2007. **80**(1): p. 194-205.
12. Alavi, S.H., et al., *Characterizing the collagen fiber orientation in pericardial leaflets under mechanical loading conditions*. Ann Biomed Eng, 2013. **41**(3): p. 547-61.
13. Schriebl, A.J., et al., *Quantitative assessment of collagen fibre orientations from two-dimensional images of soft biological tissues*. J R Soc Interface, 2012. **9**(76): p. 3081-93.
14. Pijanka, J.K., et al., *Quantification of collagen fiber structure using second harmonic generation imaging and two-dimensional discrete Fourier transform analysis: Application to the human optic nerve head*. J Biophotonics, 2019. **12**(5): p. e201800376.
15. Pourdeyhimi, B. and H. Kim, *Measuring Fiber Orientation in Nonwovens: The Hough Transform*. Textile Research Journal - TEXT RES J, 2002. **72**: p. 803-809.
16. Bayan, C., et al., *Fully automated, quantitative, noninvasive assessment of collagen fiber content and organization in thick collagen gels*. J Appl Phys, 2009. **105**(10): p. 102042.
17. Xu, S., et al., *The role of collagen in cancer: from bench to bedside*. J Transl Med, 2019. **17**(1): p. 309.
18. Püspöki, Z., et al., *Transforms and Operators for Directional Bioimage Analysis: A Survey*. Adv Anat Embryol Cell Biol, 2016. **219**: p. 69-93.
19. Wen, B., et al., *3D texture analysis for classification of second harmonic generation images of human ovarian cancer*. Sci Rep, 2016. **6**: p. 35734.
20. Meijering, E., et al., *Design and validation of a tool for neurite tracing and analysis in fluorescence microscopy images*. Cytometry A, 2004. **58**(2): p. 167-76.
21. Rubbens, M.P., et al., *Quantification of the temporal evolution of collagen orientation in mechanically conditioned engineered cardiovascular tissues*. Ann Biomed Eng, 2009. **37**(7): p. 1263-72.
22. Sun, M., A.B. Bloom, and M.H. Zaman, *Rapid Quantification of 3D Collagen Fiber Alignment and Fiber Intersection Correlations with High Sensitivity*. PLoS One, 2015. **10**(7): p. e0131814.

23. Quinn, K.P. and I. Georgakoudi, *Rapid quantification of pixel-wise fiber orientation data in micrographs*. J Biomed Opt, 2013. **18**(4): p. 046003.
24. Mori, S. and P.C. van Zijl, *Fiber tracking: principles and strategies - a technical review*. NMR Biomed, 2002. **15**(7-8): p. 468-80.
25. Bredfeldt, J.S., et al., *Automated quantification of aligned collagen for human breast carcinoma prognosis*. J Pathol Inform, 2014. **5**(1): p. 28.
26. Liu, Y., et al., *Fibrillar Collagen Quantification With Curvelet Transform Based Computational Methods*. Front Bioeng Biotechnol, 2020. **8**: p. 198.
27. Talbot, H., *A Morphological Algorithm for Linear Segment Detection*, in *Mathematical Morphology and its Applications to Image and Signal Processing*, P. Maragos, R.W. Schafer, and M.A. Butt, Editors. 1996, Springer US: Boston, MA. p. 219-226.
28. Bredfeldt, J.S., *Collagen Alignment Imaging and Analysis for Breast Cancer Classification*. 2014, The University of Wisconsin - Madison: United States -- Wisconsin. p. 152.
29. Liu, Y., et al., *Methods for Quantifying Fibrillar Collagen Alignment*. Methods Mol Biol, 2017. **1627**: p. 429-451.
30. Zeng, R., et al., *FOD-Net: A deep learning method for fiber orientation distribution angular super resolution*. Med Image Anal, 2022. **79**: p. 102431.
31. Nath, V., et al., *Deep Learning Captures More Accurate Diffusion Fiber Orientations Distributions than Constrained Spherical Deconvolution*. 2019.
32. Karimi, D., et al., *Learning to estimate the fiber orientation distribution function from diffusion-weighted MRI*. Neuroimage, 2021. **239**: p. 118316.
33. Lucena, O., et al., *Enhancing the estimation of fiber orientation distributions using convolutional neural networks*. Comput Biol Med, 2021. **135**: p. 104643.
34. Lin, Z., et al., *Fast learning of fiber orientation distribution function for MR tractography using convolutional neural network*. Med Phys, 2019. **46**(7): p. 3101-3116.
35. Lee, W., et al., *Quantitative Classification of 3D Collagen Fiber Organization From Volumetric Images*. IEEE Trans Med Imaging, 2020. **39**(12): p. 4425-4435.
36. Pham, T.T.A., et al., *Deep Learning for Analysis of Collagen Fiber Organization in Scar Tissue*. IEEE Access, 2021. **9**: p. 101755-101764.
37. Litjens, G., et al., *State-of-the-Art Deep Learning in Cardiovascular Image Analysis*. JACC Cardiovasc Imaging, 2019. **12**(8 Pt 1): p. 1549-1565.
38. Brunese, L., et al., *Deep learning for heart disease detection through cardiac sounds*. Procedia Computer Science, 2020. **176**: p. 2202-2211.
39. Chen, C., et al., *Deep Learning for Cardiac Image Segmentation: A Review*. Front Cardiovasc Med, 2020. **7**: p. 25.
40. Lu, Y., et al., *LLMScore: Unveiling the Power of Large Language Models in Text-to-Image Synthesis Evaluation*. 2023.
41. Rank, M. and A. Voigt, *Active flows on curved surfaces*. Physics of Fluids, 2021. **33**: p. 072110.
42. Sugiarto, B., et al., *Wood identification based on histogram of oriented gradient (HOG) feature and support vector machine (SVM) classifier*. 2017. 337-341.
43. Tan, L., et al., *Cardiac left ventricle segmentation using convolutional neural network regression*. 2016. 490-493.
44. Rafiq, R. and M. Albert, *Transfer Learning: Leveraging Trained Models on Novel Tasks*. 2022. p. 65-74.
45. Shuai, Y., Q. Yuan, and S. Zhao, *A Spatial-Channel Attention-Based Convolutional Neural Network for Remote Sensing Image Classification*. in *IGARSS 2022 - 2022 IEEE International Geoscience and Remote Sensing Symposium*. 2022.
46. Du, P., et al., *Advances of Four Machine Learning Methods for Spatial Data Handling: a Review*. Journal of Geovisualization and Spatial Analysis, 2020. **4**.
47. Carcagnì, P., et al., *Facial expression recognition and histograms of oriented gradients: a comprehensive study*. Springerplus, 2015. **4**: p. 645.